# Numerical simulation of dendritic growth

Y. Saito,* G. Goldbeck-Wood, and H. Müller-Krumbhaar
*Institut für Festkörperforschung der Kernforschungsanlage Jülich, Postfach 1913 D-5170 Jülich, Germany*
(Received 29 February 1988)

A one-sided diffusion-limited model for dendritic growth in two dimensions is simulated numerically by means of a Green's function in quasistationary approximation. Anisotropy in the surface tension is found necessary for dendritic growth. Scaling behavior of the growth rate and tip radius is found as function of the undercooling and anisotropy, in agreement with recent results for needle crystals. The sidebranches scale with the stability length. The numerical procedure is described in some detail.

## I. INTRODUCTION

Pattern formation and mode selection is one of the most intriguing features of nonequilibrium systems. The formation of a dendritic pattern when a crystal grows in a supercooled melt is one example of such a mode selection problem.[1,2] Ignoring surface tension, the Stefan problem of the moving interface in a diffusion field has a continuous set of steady-state shapes for a solidification front, called Ivantsov parabolas. When the surface tension is introduced, a working hypothesis of marginal stability for the selection of dendritic growth rate[1] was proposed. Even though it gave excellent agreement with experimental data, it appears to be clear by now that the growth rate selection occurs by a conceptually simpler mechanism. In contrast to the previous simplified approach, this gives a selection already for a needle crystal growing at a constant rate.

The stationary profile of the needle crystal was determined by a solvability condition at the needle tip.[3–9] By means of a Green's function the condition is formulated as a nonlinear eigenvalue problem of the growth velocity. An important new finding is the essential role of a crystalline anisotropy in capillarity. Without anisotropy in surface tension, a needle solution is unstable against tip splitting. With a nonzero anisotropy a discrete set of needle solutions is obtained.[3–8] Further stability analysis indicates that the fastest-moving solution is weakly stable against tip splitting and also against sidebranching at least for not too small values of the Péclet number. Thus it is the natural candidate for the pattern to be selected. Experiments, on the other hand, show always dendrites with sidebranches.[2,10] Accordingly, noise is assumed to trigger the sidebranch formation.

We describe in this paper a numerical simulation of the full diffusion problem in two dimensions on the one-sided model, where the diffusion takes place only in the liquid. Contrary to the previous theoretical analyses, we don't impose a needle shape to the growing crystal. The morphology as well as the growth rate of the crystal will be selected automatically in the simulation. A brief report has already been given in Ref. 11.

In Sec. II the long-range nature of the diffusion field is transformed into kernels of integral equation by means of Green's function. Discretization of the solidification front converts the one-dimensional integral equation of Sec. II into a set of linear equations in Sec. III. They are numerically solved to determine the growth rate of the solidification front, and the evolution of the front is simulated. Simulation results at various undercoolings $\Delta$ and fourfold anisotropies $\epsilon_4$ are summarized in Sec. IV. The system is always found to converge to a unique steady state where sidebranches are produced about periodically. Section V summarizes our main results.

## II. FUNDAMENTAL EQUATIONS IN TERMS OF GREEN'S FUNCTIONS

We consider an evolution of a solid-liquid interface $z(x,t)$ during the solidification of an undercooled liquid (Fig. 1). In the case where a pure substance solidifies from its melt, the process is governed entirely by thermal diffusion. If a substance solidifies from a liquid mixture, the diffusion of chemical species controls the motion of a solidification front. Both the pure thermal and pure chemical models can be treated equivalently by introducing a dimensionless diffusion field $u$,[1]

$$u=\begin{cases}(T-T_\infty)/(Lc_p^{-1}) & \text{(thermal model)} \quad (1a)\\ (\mu-\mu_\infty)/(\Delta C\,\partial\mu/\partial C) & \text{(chemical model)}\,. \quad (1b)\end{cases}$$

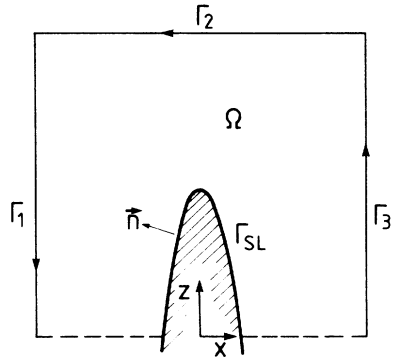


FIG. 1. Configuration of a dendrite growing in the undercooled liquid $\Omega$, enclosed by solidification front $\Gamma_{SL}$ and three boundaries $\Gamma_1(x=-\infty)$, $\Gamma_2(z=+\infty)$, and $\Gamma_3(x=+\infty)$.

 

In the thermal model $u$ is a difference of local temperature $T$ from the liquid temperature far from the interface $T_\infty$, divided by a temperature increase of the system with a specific heat $c_p$ due to the latent heat of fusion $L$. In the chemical model $u$ is the difference of a local chemical potential $\mu$ from the value far inside the liquid $\mu_\infty$, divided by a chemical potential increase due to the miscibility gap $\Delta C$ of the concentration. For a dilute solution $\mu$ can be practically replaced by $C$.

Here we consider a one-sided model corresponding to chemical diffusion, where diffusion takes place only in the liquid. The diffusion equation is written as

$$\partial u/\partial t = D\nabla^2 u \ , \tag{2}$$

with $D$ being the diffusivity. In the following we will restrict the discussion to two-dimensional diffusion. Deep inside the liquid $u$ as well as its gradient vanish. At the solid-liquid interface the diffusion field $u$ is assumed to take an equilibrium value, but with a curvature correction due to the Gibbs-Thomson effect

$$u_s = \Delta - dK \ . \tag{3}$$

Here $\Delta$ is the normalized undercooling

$$\Delta = \begin{cases} (T_M - T_\infty)/(Lc_p^{-1}) & \text{(thermal model)} \quad (4a) \\ (\mu_{\rm eq} - \mu_\infty)/(\Delta C\, \partial\mu/\partial C) & \text{(chemical model)} \ . \quad (4b) \end{cases}$$

$K$ is the local curvature of the interface, and $d$ is the anisotropic capillary length,

$$d = [\gamma(\theta) + \gamma''(\theta)] \times \begin{cases} T_M c_p L^{-2} & \text{(thermal model)} \quad (5a) \\ (\Delta C)^{-2}(\partial\mu/\partial C)^{-1} & \text{(chemical model)} \ . \quad (5b) \end{cases}$$

$T_M$ is the bulk melting temperature, $\mu_{\rm eq}$ is the equilibrium chemical potential, and $\gamma$ and $\gamma''$ are the anisotropic surface tension and its second angular derivative, respectively. When the surface tension $\gamma$ has $m$-fold crystalline anisotropy as

$$\gamma = \gamma_0[1 + \bar{\epsilon}_m \cos(m\theta)] \ , \tag{6}$$

then the capillarity length takes the form

$$d = d_0[1 - \epsilon_m \cos(m\theta)] \ , \tag{7}$$

with

$$\epsilon_m = \bar{\epsilon}_m(m^2 - 1) \ . \tag{8}$$

Note that even if the anisotropy in surface tension is small, the anisotropy in the capillarity length is enhanced; for example, with $m = 4$, $\epsilon_4$ is then 15 times larger than $\bar{\epsilon}_4$. Another boundary condition at the solid-liquid interface is the continuity condition. The latent heat $L$ or the expelled material with concentration difference $\Delta C$ is produced at a rate proportional to the growth rate of the crystal at the interface. Thus the normal velocity $v_n = (\mathbf{v}\cdot\mathbf{n})$ of the interface satisfies the continuity condition (for small supersaturations)

$$v_n = -D(\nabla u \cdot \mathbf{n}) \ . \tag{9}$$

The problem of dendritic crystal growth is to determine the profile of the solidification front and the growth velocity as a function of the undercooling $\Delta$, when all the material parameters, $L$, $c_p$, $\Delta C$, $\partial\mu/\partial C$, $D$, $T_M$, $\mu_{\rm eq}$, $\gamma_0$, and $\bar{\epsilon}_m$, are given.

In a two-dimensional system with boundary condition at $z = +\infty$ as $u(z = \infty) = 0$, the crystal grows in the positive $z$ direction with a velocity $V\hat{\mathbf{z}}$. When the crystal is growing steadily, the diffusion field satisfies a stationary equation in the moving frame of reference

$$D\nabla^2 u + V\partial u/\partial\zeta = \partial u/\partial t = 0$$

or

$$\hat{L}u = \nabla^2 u + 2l^{-1}\partial u/\partial\zeta = 0 \ , \tag{10}$$

where $\zeta$ is the new coordinate

$$\zeta = z - Vt \tag{11}$$

and $l$ is the diffusion length defined by

$$l = 2D/V \ . \tag{12}$$

Note that the boundary condition is still time dependent, as the boundary moves with locally varying velocity $v_n$ [Eq. (9)].

Practically, the crystal does not exactly grow steadily. However, when the interface moves very slowly and hence the diffusion length $l$ becomes large compared with all crystalline length scales, the interface remains effectively stationary during the time needed for relaxation of the diffusion field. In this case the problem can be solved in a quasistationary approximation: The diffusion field is obtained by solving Eq. (10) subject to the thermodynamic boundary condition (3) on the quasistationary interface, and then the explicit form of the local velocity $v(x,t)$ is found by inserting $u(x,z,t)$ into the continuity condition (9). By adjusting the velocity $V$ of the moving frame of reference to the local velocity of the crystal $v(x,t)$, especially to that at the tip of the dendrite, one can approximately obtain the asymptotic behavior of the dendritic crystal growth.

Our main problem is to solve the quasistationary diffusion equation (10). Without the Gibbs-Thomson effect or $d = 0$, the crystal takes the form of an Ivantsov parabola

$$z = -x^2/2R_0 + Vt + \text{const} \ , \tag{13}$$

which grows steadily with a tip radius $R_0$ and a velocity $V$. The Péclet number, which is the ratio of the tip radius $R_0$ to the diffusion length $l$,

$$p = R_0/l = R_0 V/2D \tag{14}$$

is determined from the undercooling $\Delta$ (in two dimensions) as

$$\Delta = \sqrt{\pi p}\, e^p \text{erfc}(\sqrt{p}) \sim \sqrt{\pi p} \quad \text{for } \Delta \ll 1 \ . \tag{15}$$

In typical experimental conditions[2] the Péclet number is small $\sim 10^{-2}$, fulfilling the necessary condition for the quasistationary approximation to hold. It is not proven

that it is a sufficient condition, but it is suggestive from the results on the boundary-layer model,[8] where part of the time dependence is kept.

The relation (15), however, determines only the ratio of $R_0$ and $V$, but cannot select a unique velocity and a radius. There is a continuous set of needle crystals with an arbitrary tip radius $R_0$ and the corresponding velocity $V=2Dp/R_0$. On the contrary, the crystal always grows with a unique velocity in the experiment for a given undercooling. Thus the selection of the final mode is governed by the capillarity.

If the capillarity effect is introduced, then the quasistationary equation (10) is no more exactly solvable analytically. We convert Eq. (10) into a one-dimensional integral equation by means of a Green's function. In the two-dimensional moving frame of reference $r=(x,\zeta)=(x,z-Vt)$, the liquid occupies the region $\Omega$ enclosed by a boundary $\Gamma$, as is shown in Fig. 1. For the quasistationary evolution $\hat{L}$ in Eq. (10) and its adjoint operator $\hat{L}^+$ are related by Green's theorem as

$$\int d\Omega(g\hat{L}u-u\hat{L}^+g)$$

$$=-\oint d\Gamma(g\partial u/\partial n-u\partial g/\partial n+2l^{-1}n_z gu)\ , \quad (16)$$

where $\mathbf{n}$ is the normal vector on the boundary $\Gamma$, directing inward into the liquid region $\Omega$. The Green's function of the adjoint operator $\hat{L}^+$ is defined as a solution of the equation

$$\hat{L}^+g(r,r')=-\delta(r-r') \quad (17)$$

and is explicitly written as

$$g(r-r')=(2\pi)^{-1}e^{(\zeta-\zeta')/l}K_0(|r-r'|/l)\ , \quad (18)$$

where $K_0$ is the modified Bessel function of the zeroth order. Inserting the solution of Eq. (10) in $u$ and the Green's function (18) in $g$, and by taking $r'$ on the boundary $\Gamma$, Green's theorem (16) reduces to the self-consistent equation for the boundary value of the diffusion field $u$ and its normal derivative $\partial u/\partial n$ as

$$c(r')u(r')=-\oint d\Gamma(g\partial u/\partial n-u\partial g/\partial n+2l^{-1}n_z gu)\ . \quad (19)$$

Here the coefficient $c(r')$ comes from the volume integration $\int d\Omega=\int dr$ of the $\delta$ function $\delta(r-r')$, which is not unity since $r'$ lies on the boundary $\Gamma$. If, for example, the boundary curve has a corner at $r'$ with angle $\varphi(r')$, then $c(r')=\varphi(r')/2\pi$. On rearranging Eq. (19), $u$ and $\partial u/\partial n$ at the boundary are related as

$$\oint d\Gamma\, g(r,r')\partial u(r)/\partial n=\oint d\Gamma\, h(r,r')u(r)\ , \quad (20)$$

where $g(r,r')$ is given in Eq. (18) and $h$ is defined by

$$h(r,r')=\partial g(r-r')/\partial n-2l^{-1}n_z g(r-r')-c(r')\delta(r-r')$$

$$=\frac{1}{2\pi l}e^{(\zeta-\zeta')/l}\left[-n_z K_0(|r-r'|/l)-\frac{n\cdot(r-r')}{|r-r'|}K_1(|r-r'|/l)\right]-c(r')\delta(r-r')\ , \quad (21)$$

where $K_1$ is the modified Bessel function of the first order. Here we note that if $u$ takes a constant value all over the boundary $\Gamma$, then $u$ remains homogeneous in the whole region of $\Omega$. Therefore, in this case the gradient $\partial u/\partial n$ vanishes at the boundary and Eq. (20) yields a condition

$$\oint d\Gamma\, h(r,r')=0\ . \quad (22)$$

In a situation where the needle or dendritic crystal is growing, the boundary consists of three lines, $\Gamma_2$ at $\zeta=\infty$, $\Gamma_1$ at $x=-\infty$ and $\Gamma_3$ at $x=\infty$, and the solid-liquid interface $\Gamma_{SL}$, as is shown in Fig. 1. On $\Gamma_{1-3}$, $u$ vanishes as well as its normal gradient $\partial u/\partial n$. Therefore, the boundary integral can be restricted on the solid-liquid interface $\Gamma_{SL}$ in Eq. (20). Condition (22), however, needs special attention. Integral contributions alongside boundaries $\Gamma_1$ and $\Gamma_3$ vanish due to the asymptotic exponential decay of the modified Bessel functions $K_0$ and $K_1$ when $x-x'$ diverges. Integrals along the boundary $\Gamma_2$ give a finite contribution

$$\lim_{\zeta\to+\infty}\int_{+\infty}^{-\infty}-dx\,[-\partial g(x-x',\zeta-\zeta')/\partial\zeta+2l^{-1}g(x-x',\zeta-\zeta')]$$

$$=\lim_{Z\to+\infty}(2\pi l)^{-1}\int_{-\infty}^{\infty}dXe^{Z/l}[K_0(\sqrt{X^2+Z^2}/l)+K_1(\sqrt{X^2+Z^2}/l)]$$

$$=\lim_{Z\to+\infty}(2\pi l)^{-1}\int dX\exp[(Z-\sqrt{X^2+Z^2})/l](2\pi l/Z)^{1/2}=\lim_{Z\to+\infty}(2\pi Zl)^{-1/2}\int dX\exp(-X^2/2Zl)=1\ . \quad (23)$$

Thus the final relation between the diffusion field $u$ and its normal derivative $\partial u/\partial n$ at the solidification front $\Gamma_{SL}$ is written as

$$\int d\Gamma_{SL}g(r,r')\partial u(r)/\partial n=\int d\Gamma_{SL}h(r,r')u(r)\ , \quad (24)$$

where $h(r,r')$ satisfies the condition

$$\int d\Gamma_{SL}h(r,r')=-1\ . \quad (25)$$

We now have basic equations (3), (9), (24), (25), (18), and (21) to describe the evolution of the solidification front in the quasistationary approximation. The scheme to perform numerical simulation is the following: For a given

velocity of the moving frame of reference $V$, the Green's function $g(r,r')$ can be calculated. If the configuration of the solidification front $\Gamma_{SL}(t)$ at time $t$ is known, $h(r,r')$ can be obtained which satisfies the condition (25). From the Gibbs-Thomson relation (3) the diffusion field along the interface $u(r)$ will be calculated. Then by solving Eq. (24) the normal gradient $\partial u/\partial n$ at the interface will be obtained. From the continuity condition (9) the normal growth velocity of the interface in the laboratory system is determined. In a short interval of time $\delta t$ the interface moves a distance $(v_n \delta t)\mathbf{n}$ in normal direction, and it now has a new configuration $\Gamma_{SL}(t+\delta t)$. In the steady growth of the crystal this quasistationary approximation is exact with $v_n=(\mathbf{V}\cdot\mathbf{n})$. Therefore, it may be appropriate to take the velocity of the moving frame $V$ to be the instantaneous velocity of the dendrite, for example, the value at the tip. In the following numerical simulation (for numerical stability) we introduce an additional kinetics for the frame velocity $V(t)$, so that it relaxes to the tip velocity of the dendrite $v_{tip}(t)$, as

$$dV/dt=-\tau^{-1}[V(t)-v_{tip}(t)] . \tag{26}$$

The numerical relaxation time $\tau$ is taken short compared with all physical time scales. This suffices to damp out fluctuations due to numerical discretization and round-off noise.

## III. NUMERICAL SIMULATION BY A BOUNDARY ELEMENT METHOD

To solve the one-dimensional integral equation (24) a boundary element method[12] is applied. The solidification front $\Gamma_{SL}$ is discretized into a polygon symmetric to the $z$ axis, whose corner points $\{r_j, j=-N,\ldots,0,1,\ldots,N\}$ have the relation $x_{-j}=-x_j$ and $\zeta_{-j}=\zeta_j$. The diffusion field $u_j$ and its gradient $q_j=\partial u_j/\partial n_j$ at a corner point $r_j$ are symmetric; $u_{-j}=u_j$ and $q_{-j}=q_j$. A point $r$ on the polygon edge $\Gamma_j$ between the corner points $r_j$ and $r_{j+1}$ is parametrized by a parameter $\xi$ between $-1$ and $+1$ as

$$\begin{aligned} r&=\phi_1(\xi)r_j+\phi_2(\xi)r_{j+1} \\ &=r_j+\phi_2(\xi)s_j=r_{j+1}-\phi_1(\xi)s_j , \end{aligned} \tag{27}$$

where

$$\phi_1(\xi)=(1-\xi)/2, \quad \phi_2(\xi)=(1+\xi)/2 \tag{28}$$

and

$$s_j=r_{j+1}-r_j . \tag{29}$$

The integration on the segment $\Gamma_j$ is written as

$$\int_{r_j}^{r_{j+1}} d\Gamma_j=(s_j/2)\int_{-1}^{1} d\xi , \tag{30}$$

where $s_j$ is the length of the line segment $s_j=|s_j|$. The curvature at $r_j$ is determined as the inverse of the radius of the circle which passes three consecutive points, $r_{j-1}, r_j, r_{j+1}$, and the normal direction $\mathbf{n}_j$ is a unit vector pointing from the center of the circle to the point $r_j$. Then for a given undercooling $\Delta$ the value of $u_j$ at the corner $r_j$ is calculated from the thermal equilibrium condition (3). The field $u$ and its derivative $\partial u/\partial n=q$ on the segment $\Gamma_j$ is approximated by the linear interpolation of the values at end points $r_j$ and $r_{j+1}$ as

$$\begin{aligned} u(\xi)&=\phi_1(\xi)u_j+\phi_2(\xi)u_{j+1} , \\ g(\xi)&=\phi_1(\xi)q_j+\phi_2(\xi)q_{j+1} . \end{aligned} \tag{31}$$

The integral equation (24) can then be written as a matrix equation

$$\sum_{j=-N}^{N} G_{ij}q_j=\sum_{j=-N}^{N} H_{ij}u_j , \tag{32}$$

where

$$\begin{aligned} G_{ij}&=(s_j/2)\int_{-1}^{1} d\xi\, g[r_j+\phi_2(\xi)s_j, r_i]\phi_1(\xi) \\ &\quad+(s_{j-1}/2)\int d\xi\, g[r_j-\phi_1(\xi)s_{j-1}, r_i]\phi_2(\xi) , \end{aligned} \tag{33a}$$

$$\begin{aligned} H_{ij}&=(s_j/2)\int d\xi\, h[r_j+\phi_2(\xi)s_j, r_i]\phi_1(\xi) \\ &\quad+(s_{j-1}/2)\int d\xi\, h[r_j-\phi_1(\xi)s_{j-1}, r_i]\phi_2(\xi) . \end{aligned} \tag{33b}$$

Integrals in Eq. (33) are performed by the four-point Gauss quadrature method.[13] When the point $r_i$ happens to be the one of the endpoints of the line segment $\Gamma_j$ where the integrations are performed, we have to be careful on the logarithmic singularity of the Green's function for a short separation $|r-r'|$ as

$$g(r,r')\sim \exp[(\xi-\zeta')/l]\{-\ln[|r-r'|/2l]-\gamma\} , \tag{34}$$

where $\gamma$ is an Euler constant $\gamma=0.5772\cdots$. In the relevant calculation of $G_{ij}$ and $H_{ij}$ with $j=i$ and $i\pm1$ we use the Gaussian integration for integrands with a logarithmic singularity.[13]

The condition (25) on the integral kernel $h$ reduces to the one on $H$ as

$$\sum_{j=-N}^{N} H_{ij}=-1 \tag{35}$$

from which the diagonal element $H_{ii}$ is determined as

$$H_{ii}=-\sum_{j(\neq i)} H_{ij}-1 . \tag{36}$$

The linear equation (32) is solved to give the gradient $q_j=\partial u_j/\partial n_j$ at a corner point $r_j$, which then determines the local normal velocity $v_{n,j}$ through Eq. (9). The solidification front moves $-Dq_j\mathbf{n}_j\,\delta t$ in a short interval of time $\delta t$. The time increment $\delta t$ here is chosen small enough to avoid numerical instabilities. The velocity of the moving frame $V$ is adjusted to the growth rate of the crystal, typically to the tip velocity $v_{tip}$ by the relaxation equation (26). We repeat this procedure to simulate the growth of the solidification front.

Our main interest lies in the evolution of the dendrite tip, and we have to introduce some cutoff at a finite height. In order to lessen the effects of finite size on the

evolution of the dendrite tip, we have divided the interface into three parts along $z$: a tip region, a transition region, and a tail region. The tip region has a predetermined height which accomodates at least three side-branches from the top. Here the evolution is fully treated as described above. The grid spacings $s_j$ are dynamically adjusted at each time step to fall in an interval

$$s_{\max}/2 < s_j < s_{\max} .$$

If a length of a segment $\Gamma_j$ exceeds $s_{\max}$, a corner point is added in the middle of an averaged arc joining $r_j$ and $r_{j+1}$. If two consecutive points become too close, one of them is eliminated. After the addition or elimination of points, all separations are equilibrated by diffusing the grid points along the interpolated surface. For a dendrite with a tip radius $R$, $s_{\max}$ is chosen to be about $0.03R \sim 0.11R$, and the typical grid spacing $s_j$ is smaller than $0.05R$.

When the dendrite is cut off at a finite height, the cutoff effect extends about a diffusion length $l$. Thus we have to set a cutoff far down from the tip in order to suppress its effect on the growth rate and patterns of dendrite tip. Since the growth rate of the dendrite may primarily be governed by the dendrite tip, the detailed structure of the tail presumably can be neglected. (This will be justified below.) We thus assume a long and smooth tail. As we know that the stationary smooth interface which satisfies the continuity condition (9) is just the Ivantsov parabola, the tail is assumed to take the form of the Ivantsov parabola (13) with velocity $V$. Its radius parameter $R_0$ is determined by $V$ and $\Delta$, or the Péclet number $p$ given in Eq. (15) from the relation (14). The extent of the tail region is more than five times the diffusion length $l$, which turned out to be long enough to suppress any appreciable finite-size effect in the growth of the dendrite tip. Between the tip and the tail regions, there is an intermediate transition region with a predetermined width. The transition region is the end of the tip region, whose motion is essentially frozen with a small modification in order to connect the tip and tail regions smoothly. It is discretized as fine as the tip region, whereas the discretization in the tail region coarsens gradually down along the tail. The transition and tail regions are taken into account in solving the linear equation (32) to obtain the growth rate of the tip region, but their evolutions are not governed by this solution.

In order to test the validity of the numerical simulation, we have calculated normal velocities $v_n$ along an Ivantsov parabola for $d_0=0$, where an exact solution is known. In the whole tip region the relative precision is better than $5\times10^{-4}$, indicating also that the cutoff effect is well suppressed in the tip region. The main effect of the tail is to guarantee the global conservation of $u$ which is exploited in the derivation of (25) and (35). Finally, this set of numerical boundary conditions allows us to grow dendrites over arbitrary amounts of time.

## IV. RESULTS

Succinonitrile is the substrate whose dendritic growth is most intensively investigated in experiment.[2] The capillary length $d_0$ of this substance is $2.86\times10^{-7}$ cm, and for the supercooling $\Delta=0.2$ the ratio of the capillarity length $d_0$ to the diffusion length $l=2D/V$ is about $5\times10^{-4}$ and the ratio of $d_0$ to the tip radius $R$ is about $7\times10^{-3}$. Even though these ratios are obtained in three-dimensional experiments, the same order of proportionality may be expected in two dimensions. For convenience we choose our unit of length as $d_0=10^{-3}$, expecting $l$ to be of order 10 and $R$ of order unity at $\Delta=0.25$. The discretization parameter $s_{\max}$ is chosen about one-tenth of the radius to be $s_{\max}\leq0.1$. With larger undercooling $\Delta=0.5$ the dendrite grows faster with a sharper tip. Therefore we choose a smaller $s_{\max}$ to be $\leq0.02$. Corresponding also to succinonitrile, a four-fold anisotropy is assumed with an anisotropy coefficient in the capillarity length $\epsilon_4=0$, 0.05, 0.10, and 0.15 (or the one in surface tension $\tilde{\epsilon}_4=0$, 0.0033, 0.0067, and 0.01, respectively).

Figure 2 shows the evolution of a dendritic crystal with an anisotropy $\epsilon_4=0.10$ at an undercooling $\Delta=0.25$. The left-hand side in growth direction shows the tip region only, whereas the right-hand side includes the transition region. The initial configuration was the Ivantsov parabola (13) with an initial velocity $V_i=0.097$ (or $l_i=20.6$). Since the Péclet number for this undercooling $\Delta=0.25$ is $p=2.86\times10^{-2}$, the initial curvature at the tip is $K_i=1.70$ and correspondingly the radius is $R_i=0.589$. The tip region has a height $h=25$, and the tail has initially a length $5l_i\cong100$ with a transition region of width 5 in between. The tip region is discretized with a maximum separation $s_{\max}=0.1$, and there are about 400 points in one side of the tip region. As the system evolves, the coarse-grained velocity decreases to approach an asymptotic steady-state velocity $V=0.059$ (or $l=33.9$). (For $\Delta=0.5$ the behavior is completely analogous, as shown in Fig. 3). The selected value of the growth rate does not depend on the initial configuration of the crystal. For example, in another simulation with an initial velocity $V_i=0.04$ and a tip radius $R_i=1.428$, the same steady-state profile of the dendrite is obtained. This steadily growing dendrite resembles globally an Ivantsov parabola with the same undercooling $\Delta=0.25$ and the velocity $V=0.059$. (See Fig. 2. A more detailed comparison is made in Fig. 4 for $\Delta=0.5$.) Locally, however, there are differences. The radius at the dendrite tip $R=0.085$ is smaller than the Ivantsov value $R_0=0.968$ calculated from Eq. (14) by a factor $R/R_0=0.914$ but this small difference directly at the tip is practically invisible. In order to keep up the same velocity, the crystal with a finite surface tension should have a dendrite tip sharper than the one without a surface tension. Coming down from the tip, the separation $w$ between the dendrite and the associated Ivantsov parabola oscillates as does the local curvature of the dendrite. From Figs. 2 and 4 a side-branch becomes visible at about a distance $3R$ from the tip, and has a periodicity $\lambda$ of about $3R$ at $\epsilon_4=0.1$.

On increasing the undercooling, for example to $\Delta=0.5$, a dendrite with an anisotropy $\epsilon_4=0.09$ grows fast with $V=1.79$ and the tip becomes sharp in the steady state. The fine discretization is chosen as

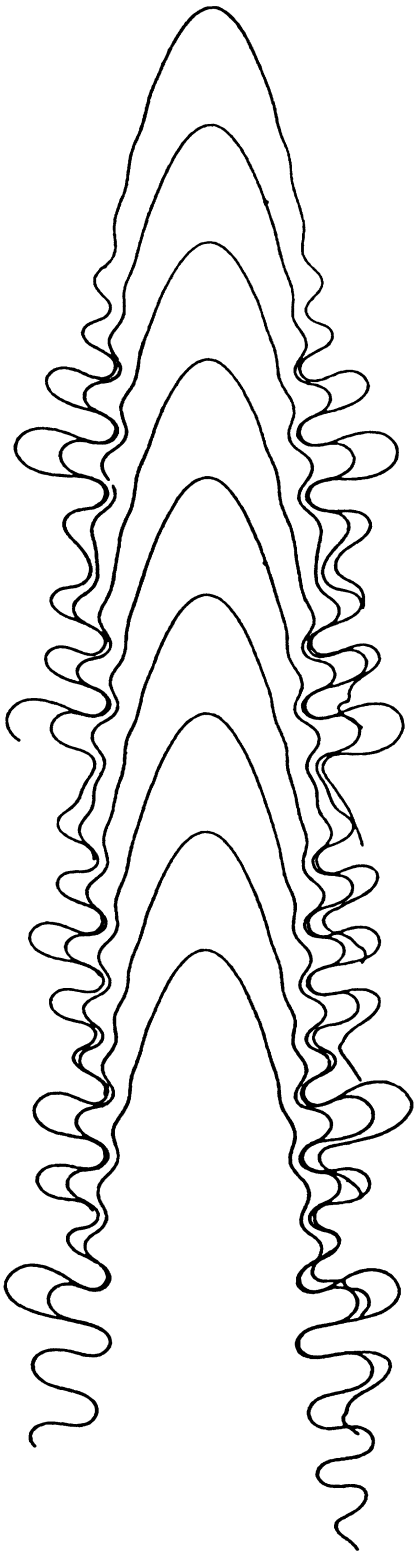

FIG. 2. Stroboscopic plot of the evolution of a dendritic crystal at an undercooling $\Delta=0.25$ with an anisotropy in the capillarity $\epsilon_4=0.10$. The tip region has a height $h=25$ with a discretization parameter $s_{\max}=0.10$ in a unit where the capillarity length $d_0=0.001$. In the steady state, the diffusion length becomes $l=2D/V=34$ and the tip radius is $R=0.885$.

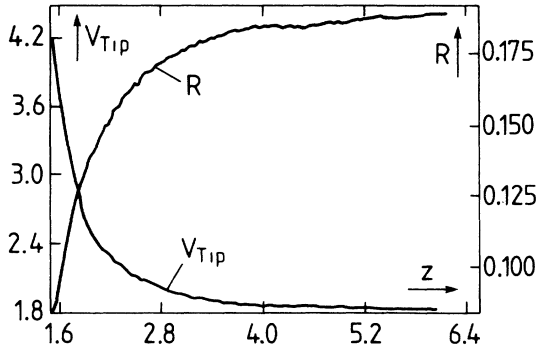


FIG. 3. Temporal variations of the velocity and the tip radius of the dendrite shown in Fig. 5(b).

$s_{\max}=0.02$, compared with the final tip radius $R=0.19$. The large growth rate means a short diffusion length $l\sim 1.1$. In this case we have initially tried another boundary condition. Instead of the transition and the tail regions, we set flat wings at the foot of the dendrite, where the boundary condition is kept $u=\Delta$. (See Fig. 5.) This corresponds to the growth of a dendrite starting from an extrusion of a flat solid-liquid interface.[14] When the height of the dendrite is less than the diffusion length $l$, the tip is influenced from the tail or wing structure. When the dendrite grows far enough, the tail effect does not play a role, and the final velocity and the profile of the dendrite turns out to be independent of the boundary condition at the foot of the dendrite. For small undercooling as $\Delta=0.25$, however, the latter growth simulation out of an extrusion from the flat interface is impossible because the height and the corresponding number of polygonal corner points become too large before the dendrite settles to a stationary velocity.

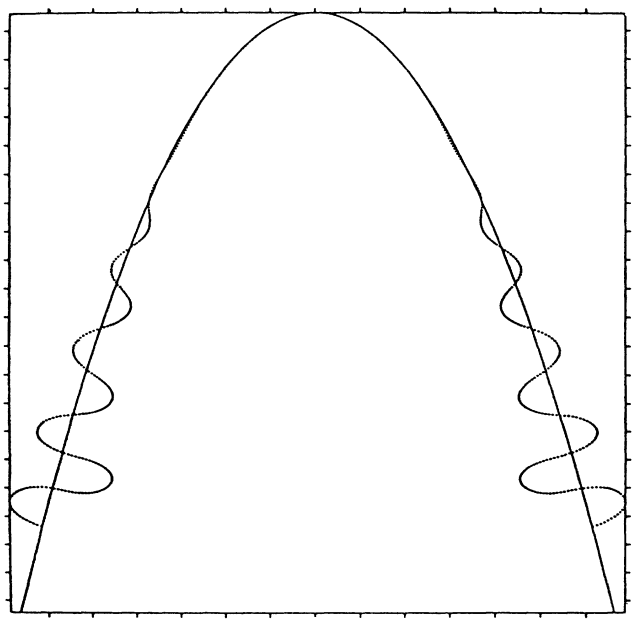

FIG. 4. Final profile of the dendrite tip compared with a corresponding Ivantsov parabola.

Now we vary the anisotropy parameter $\epsilon_4$. Without the surface anisotropy, $\epsilon_4=0$, the initial parabola becomes deformed, as depicted in Fig. 6. The tip velocity decreases monotonically in time, and the tip radius increases. This means the curvature decreases and it may eventually turn negative and result in a tip splitting. For nonzero anisotropies, as $\epsilon_4=0.05$, 0.10, 01.5, and 0.20 for $\Delta=0.25$ and $\epsilon_4=0.048$, 0.091, 0.13, and 0.167 for $\Delta=0.5$, the dendrite converges to a stationary sidebranch-producing profile. Figure 7 shows the scaled growth rate

$$\sigma=Vd_0/2Dp^2=2Dd_0/VR_0^2 \tag{37}$$

versus the anisotropy coefficient $\epsilon_4$. Here $p$ is the Péclet number (13) determined from the undercooling $\Delta$, and $R_0$ is the inverse curvature at the tip of the Ivantsov parabola growing with velocity $V$. In the limit of small undercooling $\Delta$, the marginal stability hypothesis[1] predicted that $\sigma$ in the steady state takes a universal constant $\sigma^*$, independent of the undercooling. Our simulation shows that $\sigma$ depends on the anisotropy $\epsilon_4$ but it is essentially independent of the undercooling $\Delta$. From the weak dependence of the growth rate on the discretization $s_{\max}$ (as we have studied systematically) one can extrapolate the velocity $V$ at $s_{\max}\to 0$. These extrapolated values falls on a dashed curve in Fig. 7. In the small undercooling limit where $\Delta\sim\sqrt{\pi p}$, the scaled growth rate reduces to

$$\sigma=\pi^2Vd_0/2D\Delta^4=8/C\ . \tag{38}$$

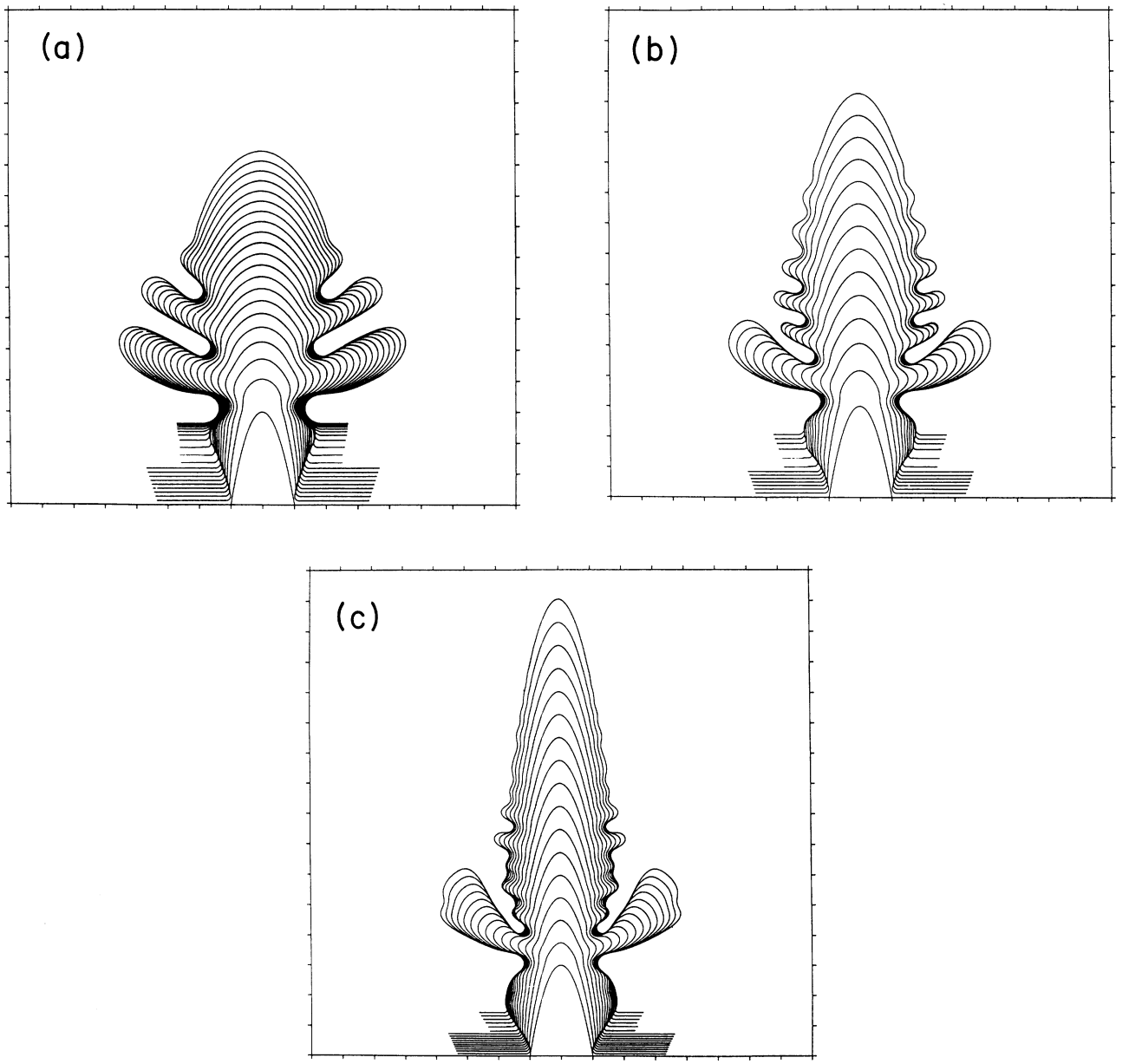


FIG. 5. (a)–(c) Dendrite crystal grown from an initial extrusion in a flat interface at $\Delta=0.5$ and $\epsilon_4=0.048$, 0.091, 0.167.

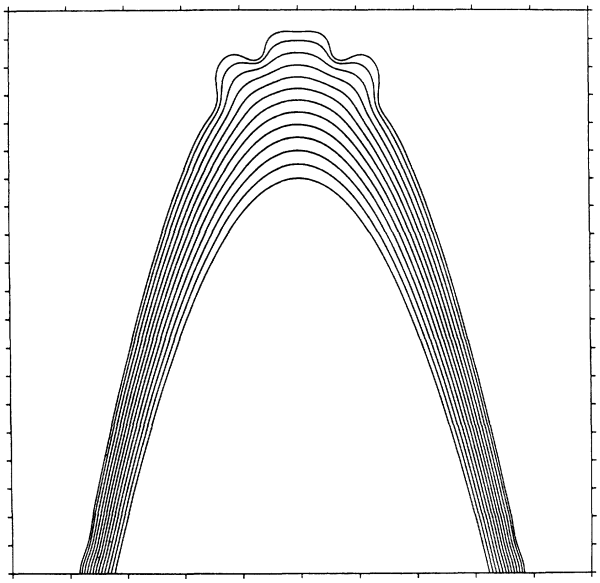

FIG. 6. Tip splitting of a needle crystal at $\epsilon_4=0$.

Here $C=16D\Delta^4/\pi^2 d_0 V$ is the nonlinear eigenvalue of the symmetrical model treated by Pelce and Pomeau[3] and Ben Amar and Pomeau and Ben Amar and Moussallam.[7,9] Both the raw data and the extrapolated curves of the scaled growth rates are proportional to the corresponding value $8/C$ calculated by Ben Amar and Moussallam.[9] A recent calculation[15] for the one-sided needle crystal gives the same scaling behavior as (37), with $\sigma$ being larger by a factor of 2. Note that our data do not satisfy the asymptotic form (38) but (37), where $\Delta$ is transformed into $p(\Delta)$, as $\Delta$ is not really small here. Thus the velocity $V$ in units of $2D/d_0$ is a multiple of two constant factors, $\sigma$, which depends only on the anisotropy $\epsilon_4$, and $p^2$, which depends only on the supercooling $\Delta$:

$$V=(2D/d_0)\sigma(\epsilon_4)p(\Delta)^2 , \tag{39}$$

where $p(\Delta=0.25)=0.0286$ and $p(\Delta=0.5)=0.187$.

The actual Péclet number $P$ defined as the ratio between the tip radius $R$ and the diffusion length $l=2D/V$ differs from its Ivantsov value $p(\Delta)$ determined only from the undercooling $\Delta$ by Eq. (13). Their ratio $\rho=P/p(\Delta)=R/R_0$ depends on the anisotropy $\epsilon_4$ but is almost independent of the undercooling $\Delta$, as is shown in Fig. 8. Therefore the tip radius is given by

$$R=(2D/V)\rho(\epsilon_4)p(\Delta)=d_0\rho/\sigma^2 p(\Delta) . \tag{40}$$

Equations (39) and (40) yields the universal combination of the actual growth rate $V$ and the tip radius $R$ as

$$2Dd_0/RV^2=\sigma/\rho^2 , \tag{41}$$

which is only the function of an anisotropy $\epsilon_4$, as is plotted in Fig. 9. This quantity is in fact measured in the experiment and is found to be essentially independent of the supercooling $\Delta$.[2] Experiments, however, are performed in three dimensions. The fact that the scaling result (37) appears to hold both in two and in three dimensions can be attributed to the fact that dimensionality enters in the relation $p(\Delta)$, while the scaling (37) then contains relations between length and time scales only.

The next quantity to be discussed is the wavelength of the sidebranches. We have defined the inverse wavelength $\lambda^{-1}$ as the number of sidebranches produced per time unit, divided by the growth rate $V$. This encompasses the difficulty to decide along which direction the wavelength is to be measured and is insensitive (albeit not completely independent) to the coarsening of sidebranches further down the shaft. The marginal stability hypothesis[1] predicted a scaling

$$\lambda \gtrsim \lambda_s=2\pi\sqrt{ld_0}=2\pi R_0\sqrt{\sigma} , \tag{42}$$

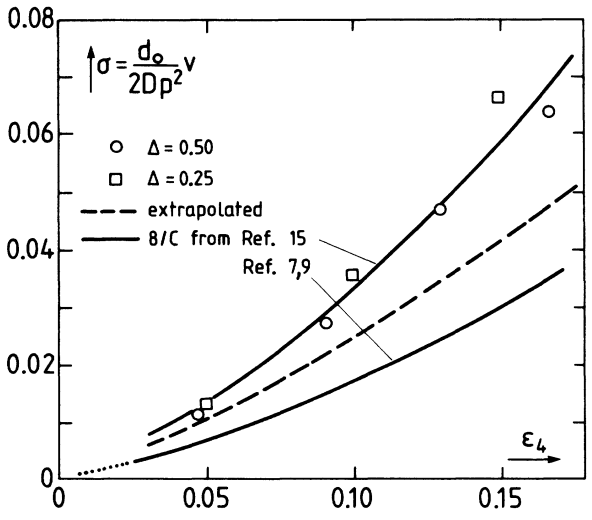


FIG. 7. Normalized growth rate $\sigma=Vd_0/2Dp^2$ versus anisotropy parameter $\epsilon_4$ for $\Delta=0.25$ and 0.5. The dashed line is our extrapolation to zero grid spacing $s_{\max}\to 0$; the solid curve correspond to the needle solutions.

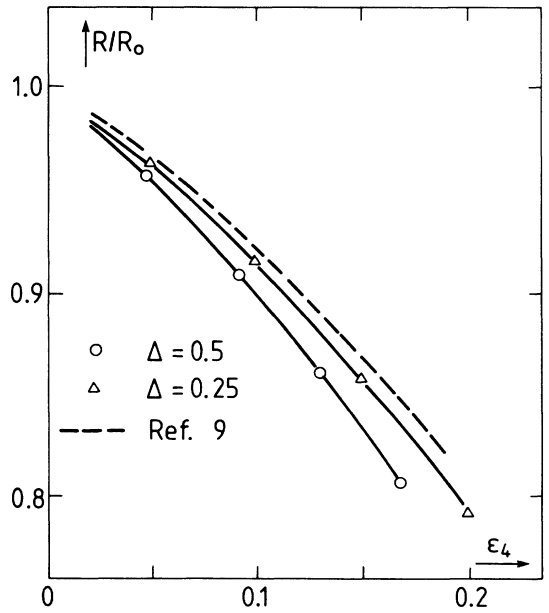


FIG. 8. Ratio of the tip radius $R$ to the Ivantsov value $R_0$ as a function of anisotropy parameter $\epsilon_4$.

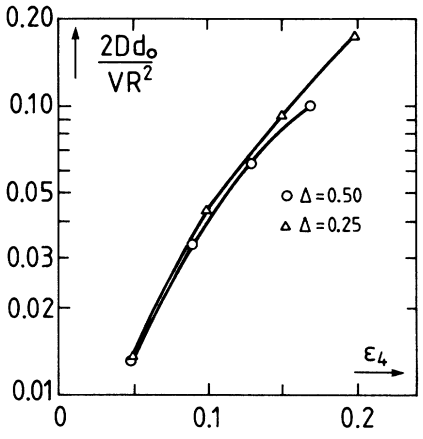


FIG. 9. Scaling behavior of $VR^2$.

with the stability length $\lambda_s$. More recent asymptotic analyses[16,17] for the evolution of a wave packet based on the microscopic solvability confirm this scaling with $\sqrt{\sigma}$, at least at a fixed distance from the tip.

Our numerical results are shown in Fig. 10, where scaling like (42) would correspond to a horizontal line, independent of $\Delta$ and $\epsilon_4$. This is apparently well confirmed, agrees qualitatively with linear stability calculations[18] on the symmetrical model, and even agrees with experiments[2] in three dimensions at fixed $\epsilon_4 \approx 0.1$ where a relation $\lambda = 3R_0$ was reported. One should note, however, that $\epsilon_4$ is largely determined by the angular derivative (5) of the surface tension (stiffness), which until now cannot be determined accurately from experiments.

A final point concerns the influence of noise. Stability analyses[6,16–18] of the needle crystal show it to be weakly stable against sidebranch formation. Under (say, thermal) noise at the tip these weakly stable modes are excited at the tip and then grow over some distance in space, down the shaft of the needle. This leads to an effective amplification of noise[6,16–18] and hence to some irregularity in the sidebranch pattern, as also observed experimentally.

A precise quantification of this noise effect is difficult both numerically and experimentally. As soon as the amplitude of the sidebranches is an appreciable fraction of their wavelength, they start to compete via the diffusion field which leads to coarsening in a somewhat random fashion. This irregularity is coupled back to the tip via the diffusion field and could eventually provide a self-triggering of noise at the tip. We see such an effect when we set our boundary between the tip and the tail further down the shaft, as it slightly reduces the average amplitude of the sidebranches near the tip. A crucial test, however, would require an extrapolation of numerical noise to zero. With our present integration scheme this does not look feasible, but an improvement seems possible if one would explicitly treat the deviation of the dendrite from the smooth needle form only.

Experimentally one is in a rather similar situation. The amplitudes of the sidebranches appear to increase with decreasing size of the dendrite.[2] In other words, the effect of thermal noise should be relatively small for large dendrites, but the diffusion length according to (37) increases quadratically with the size of the dendrite and hence the size of the container sets an upper limit.

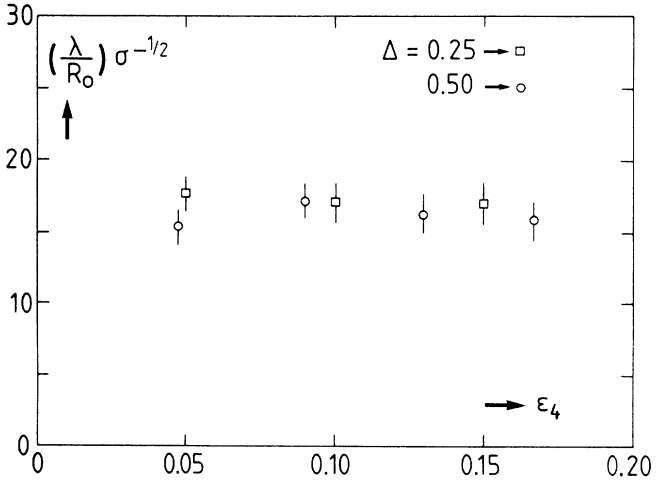


FIG. 10. Scaled wavelength vs anisotropy for two different supercoolings.

## V. CONCLUSION AND DISCUSSION

Diffusion-controlled dendritic growth has been simulated numerically in quasistationary approximation. This quasistatic approximation is expected to be good in the experimentally most interesting range of small supercooling, $\Delta \lesssim 0.5$. The length of the dendrite considered is restricted to a few sidebranches away from the tip plus an averaging procedure over a long tail to ensure global conservation laws. This restriction—in comparison with real experiments—fortunately did not appear to be crucial for the questions of interest here. On the other hand, the numerical scheme described here gives full control over the important parameters like surface tension and anisotropy.

For a given undercooling, the system converges to a unique quasisteady state where sidebranches are produced about periodically. The growth rate $V$ and the tip radius $R$ satisfy the relation (41), and the combination $VR^2$ depends only on the strength of the anisotropy $\epsilon_4$, but is independent of the undercooling $\Delta$, in agreement with experiments. The growth rate $V$ itself depends on both $\epsilon_4$ and $\Delta$ by a scaling relation. The dimensionless growth rate $V/(2D/d_0)$ is factorized into a product of functions of $\epsilon_4$ and $\Delta$ as in Eq. (39). The basic scaling function $\sigma = Vd_0/2Dp(\Delta)^2$ is given in Eq. (37) and shows a dependence on $\epsilon_4$ quite similar to the prediction for the smooth needle crystal, as is shown in Fig. 7. Our numerical simulation yields also a scaling behavior in the tip radius $R$. The dimensionless radius $R/d_0$ is factorized into functions of $\epsilon_4$ and $\Delta$, as is represented in Eq. (40). Furthermore we confirm scaling, Eq. (42), of the spacing between sidebranches $\lambda \gtrsim \lambda_s$, in agreement with the experiments on different materials.

These results are remarkable, insofar as the pattern in Fig. 3 with the sidebranches is very different from the needle solution. The quantitative agreement indicates that the selection process here is largely governed by the immediate neighborhood of the tip. Our results concerning the influence of noise on the formation of sidebranches are qualitatively consistent with recent predictions from the linearized theory,[6,16–18] but more work is needed to draw a quantitative conclusion on this point. Finally, kinetic anisotropy could also easily be included in our scheme, but since no experimental data exist we also leave this to the future.

## ACKNOWLEDGMENT

We thank Martine Ben-Amar, Christiane Caroli, and Bernard Caroli for valuable discussions.

*Permanent address: Department of Physics, Keio University, 3-14-1 Hiyoshi, Kohoku-Ku, Yokohama, Japan.

[1]J. S. Langer, Rev. Mod. Phys. **52**, 1 (1980); J. S. Langer and H. Müller-Krumbhaar, Acta Metall. **26**, 1681 (1978); **26**, 1689 (1978); **26**, 1697 (1978); H. Müller-Krumbhaar and J. S. Langer, *ibid.* **29**, 145 (1981).

[2]M. E. Glicksman, R. J. Schaefer, and J. D. Ayers, Metall. Trans. **7A**, 1747 (1976); S. C. Huang and M. E. Glicksman, Acta. Metall. **29**, 701 (1981); **29**, 717 (1981).

[3]P. Pelce and Y. Pomeau, Studies Appl. Math. **74**, 1283 (1986).

[4]B. Caroli, C. Caroli, B. Roulet, and J. S. Langer, Phys. Rev. A **33**, 422 (1986); A. Barbieri, D. C. Hong, and J. S. Langer, *ibid.* **35**, 1802 (1987).

[5]D. Kessler, J. Koplik, and H. Levine, in *Pattern, Defects and Microstructures in Nonequilibrium Systems,* edited by D. Walgraef (Martinus Nijhoff, Dordrecht, 1987); D. Kessler and H. Levine, Phys. Rev. A **33**, 2621 (1986); **33**, 2634 (1986).

[6]D. Kessler and H. Levine, Phys. Rev. A **33**, 7867 (1986).

[7]M. Ben-Amar and Y. Pomeau, Europhysics Lett. **2**, 307 (1986).

[8]E. Ben-Jacob, N. Goldenfeld, J. S. Langer, and G. Schön, Phys. Rev. Lett. **51**, 1930 (1983); Phys. Rev. A **29**, 330 (1984).

[9]M. Ben-Amar and B. Moussallam, Physica **25D**, 155 (1987).

[10]H. Honjo, S. Ohta, and Y. Sawada, Phys. Rev. Lett. **55**, 841 (1985).

[11]Y. Saito, G. Goldbeck-Wood, and H. Müller-Krumbhaar, Phys. Rev. Lett. **58**, 1541 (1987).

[12]C. A. Brebbia, *The Boundary Element Method for Engineers* (Penetech, London, 1978).

[13]*Handbook of Mathematical Functions,* edited by M. Abramowitz and I. A. Stegun (Dover, New York, 1972), p. 875.

[14]G. Goldbeck-Wood, master thesis, Rheinisch-Westfälische Technische Hochschule Aachen, 1986; H. Müller-Krumbhaar, G. Goldbeck-Wood, and Y. Saito, in Proceedings of the OJI Seminar on Crystal Morphology and Growth Units, Yamagata, Japan, 1985 (unpublished).

[15]C. Misbah, J. Phys. **48**, 1265 (1987).

[16]B. Caroli, C. Caroli, and B. Roulet, J. Phys. **48**, 1423 (1987).

[17]M. N. Barber, A. Barbieri, and J. S. Langer, Phys. Rev. A **36**, 3340 (1987).

[18]D. Kessler and H. Levine, Phys. Rev. Lett. **57**, 3069 (1986); unpublished.